# Application of Omega-Liutex Identification Method in the Cavitating Flows Around a Three-Dimensional Bullet

**Chapter** · January 2021

DOI: 10.1007/978-3-030-70217-5_25

CITATIONS
0

READS
91

**4 authors:**

Rundi Qiu
Chinese Academy of Sciences
**3** PUBLICATIONS **3** CITATIONS
SEE PROFILE

Renfang Huang
Chinese Academy of Sciences
**39** PUBLICATIONS **323** CITATIONS
SEE PROFILE

Yiwei Wang
Chinese Academy of Sciences
**84** PUBLICATIONS **643** CITATIONS
SEE PROFILE

Chenguang Huang
Chinese Academy of Sciences
**207** PUBLICATIONS **1,680** CITATIONS
SEE PROFILE

# Chapter 25
# Application of Omega-Liutex Identification Method in the Cavitating Flows Around a Three-Dimensional Bullet


**Rundi Qiu, Renfang Huang, Yiwei Wang, and Chenguang Huang**

**Abstract** The objectives of this paper are (1) to provide a better insight into the dynamics and structures of transient cavitation, and (2) to better understand the interaction between unsteady cavitating flow and vortex dynamics using different vortex-identification methods. Numerical simulations of unsteady cavitating flows are conducted around a three-dimensional bullet using Large Eddy Simulation (LES) method via the open-source code, OpenFOAM. The results reliably predict unsteady cavitation patterns, including cavity initiation, growth, and collapse in a short time. To clarify the mechanism of cavitation-vortex interaction, the Omega-Liutex method is used to visualize vortex structure. The results show strong correlations between a cavity and vortex structure.

**Keywords** Transient cavitation · OpenFOAM · Vortex identification · Omega-Liutex

R. Qiu
Key Laboratory for Mechanics in Fluid Solid Coupling Systems, Institute of Mechanics, Chinese Academy of Sciences, Beijing, China

School of Future Technology, University of Chinese Academy of Sciences, Beijing, China
e-mail: qiurundi19@mails.ucas.edu.cn

R. Huang (✉)
Key Laboratory for Mechanics in Fluid Solid Coupling Systems, Institute of Mechanics, Chinese Academy of Sciences, Beijing, China
e-mail: hrenfang@imech.ac.cn

Y. Wang · C. Huang
Key Laboratory for Mechanics in Fluid Solid Coupling Systems, Institute of Mechanics, Chinese Academy of Sciences, Beijing, China

School of Future Technology, University of Chinese Academy of Sciences, Beijing, China

School of Engineering Science, University of Chinese Academy of Sciences, Beijing, China
e-mail: wangyw@imech.ac.cn; huangcg@imech.ac.cn



C. Liu, Y. Wang (eds.), *Liutex and Third Generation of Vortex Definition and Identification*, https://doi.org/10.1007/978-3-030-70217-5_25

## 1 Introduction

Cavitation is a common hydrodynamic phenomenon which usually occurs where the speed of water is high enough. When local pressure is lower than saturated vapor pressure, water turns into vapor and copious bubbles are generated. The collapse of bubbles increases the fluctuation of the pressure field in a short time, which can greatly reduce hydraulic mechanical performance. Compared with general hydrodynamic phenomena, cavitation has unique characteristics, including a shorter characteristic time and a free surface, neither of which can be predicted. These characteristics result in difficulties in obtaining a theoretical solution about cavitation. Thus, numerical simulation has become an effective method in exploring the properties of cavitation.

The presence of unsteady cavitating flow is accompanied by complex vortex formation and elimination. How to show the process of vortex motion is a vital issue in a numerical simulation of cavitation. Initially, such a simulation was based on the Reynolds averaged Navier–Stokes equations (RANS). Coutier-Delgosha et al. [1] compared the influences on the numerical results of four turbulence models based on RANS. The result showed that standard $k-\varepsilon$ and standard $k-\omega$ models are unable to predict cavity shedding. After these models were corrected by including turbulent viscosity, the simulation results agreed well with experiment. With increases in computing speed, large eddy simulations (LES) are gaining increased attention. Compared with RANS, LES can resolve vortex structure more accurately. Therefore, LES are more suitable for cavitating flows with complex vortex motion. Dittakavi et al. [2] used LES to calculate cavitating flow in a Venturi tube. They pointed out that LES can describe vortex structure more clearly than RANS, and they derived the law of vorticity transport. Roohi et al. [3] applied LES to a two-dimensional Clark-Y hydrofoil cavitating flow. They indicated that LES predicted the shape of cavitation more accurately than RANS, even if the mesh did not strictly comprise two-dimensional grids. LES performed equally well in three dimensions. Nowadays, it is common to use the LES method for high-fidelity simulations of cavitating flows.

The interactions between vortices have a significant effect on the dynamics of cavitation flow. For the unsteady cavitation of a hydrofoil, cavity instability originates from the mechanism of the re-entrant jet [4]. At the cavitation-shedding stage, the re-entrant jet creates numerous vortices of different sizes in a fluid. How to identify and analyze vortex structure is helpful in exploring cavitation characteristics. An understanding of vortices broadly derives from a strict mathematical definition. Helmholtz proposed the concepts of vorticity tubes/filaments [5]. Based on the definition of a vortex, three vortex theorems can be derived, which provides a basis for detailed analysis of vortex structures. However, vorticity cannot distinguish between the rotation area and the shear area. Although the mathematics of vorticity are clear and easy to use, they are not suitable for cavitating flow. To clarify the physical meaning of a vortex, researchers have constructed a second-generation vortex definition method based on eigenvalues, including the Q criterion [6], the

Δ criterion [7], and the $\lambda_2$ criterion [8]. These criteria have appropriate physical meaning and can distinguish rotation from shear in a flow field. Nevertheless, due to its very definition, a vortex structure selected using various criteria is subjective. Different parameters in the criteria lead to different results and various vortex structures, and there is no general agreement on vortex identification. To solve these problems, Liu et al. have developed a new identification method for vortices to overcome the disadvantages inherent to traditional methods. They proposed the Omega vortex-identification method [9–11]. Based on this method, Dong et al. created a new method named Omega-Liutex [12]. By normalizing the value of a criterion to a value between 0 and 1, Omega and Omega-Liutex reflect the shape of the vortex structure objectively. They claim that this is a third-generation vortex-identification method, which performs well in different cases; and that it is a reliable tool for analyzing the characteristics of a vortex. Wang et al. [13] investigate the turbulent drag reduction mechanism by analyzing the characteristic of vortex structure in the viscoelastic turbulent flows, and they compared various vortex identification method. Researchers improve Omega-Liutex method and obtain Rortex method, which is helpful to identify the vortex line and vortex core [14–16].

The vortex-identification method has wide application prospects in the field of cavitating flow, because the cavitation dynamics is closely related to the evolution of cavitation vortex structures. Wang et al. [17] compare different vortex identification method in cavitation vortex dynamics and show the performances of various methods in identifying cavitation vortex structures. Studies on water pumps [18] and turbine [19] have been conducted in recent years, but related research in hydrodynamics is still to be developed. The focus of this work is on investigating the interaction between a vortex and transient cavitation. We simulate a three-dimensional cavitating flow around a bullet using LES turbulence and a Schnerr–Sauer cavitation model. The volume fraction of the water phase is used to analyze cavitation-shape evolution over time. The wake flow of the bullet is used to observe the characteristics of fluid motion. To obtain a clear vortex structure, the Omega-Liutex identification method is utilized to analyze the flow field around the bullet. We hope our work will provide a reference for the application of Omega-Liutex in three-dimensional problems in actual engineering structures.

## 2 Numerical Methods and Computation Setting

In this paper, the flow field around the bullet is obtained by solving a discrete Navier–Stokes equation. Multiphase flow cavitation theory can be used to calculate the interface between the vapor and liquid. In general, the cavitation-flow regime is regarded as a homogeneous bubbly flow. The continuity equation and momentum equation are simplified for a single-phase flow scenario. According to the above assumptions and conditions, the expression for the phase transition is achieved using a cavitation model of the transport-equation type. The phase transition

between gas and liquid follows the rule of mass transfer. So, the mass conservation equation can be obtained:

$$\frac{\partial \rho}{\partial t} + \nabla \cdot (\rho \mathbf{U}) = \dot{m}^{+} - \dot{m}^{-} \tag{25.1}$$

α, ρ, **U**, $\dot{m}^{+}$, $\dot{m}^{-}$ represent the volume fraction, effective mixture density, velocity vector, evaporation rate, and the condensation rate, respectively. The effective mixture density in homogeneous bubbly flow is defined as:

$$\rho = \alpha_l \rho_l + \alpha_v \rho_v \tag{25.2}$$

where the subscripts l and v represent the vapor phase and the liquid phase, respectively. Different expressions for $\dot{m}^{+}$ and $\dot{m}^{-}$ are derived for different cavitation models. In this paper, the Schnerr–Sauer cavitation model is proposed to simulate the process of evaporation and condensation. $\dot{m}^{+}$ and $\dot{m}^{-}$ are defined as follows:

$$\dot{m}^{+} = C_e \frac{3\rho_l \rho_v \alpha_l (1-\alpha_l)}{\rho R_b} \sqrt{\frac{2}{3} \frac{\max(p_{sat} - p, 0)}{\rho_l}} \tag{25.3}$$

$$\dot{m}^{-} = C_c \frac{3\rho_l \rho_v \alpha_l (1-\alpha_l)}{\rho R_b} \sqrt{\frac{2}{3} \frac{\max(p - p_{sat}, 0)}{\rho_l}} \tag{25.4}$$

$$R_b = \left( \frac{1-\alpha_l}{\alpha_l} \frac{3}{4\pi n} \right)^{\frac{1}{3}} \tag{25.5}$$

$p_{sat}$ is the saturated vapor pressure, $R_b$ is the radius of a bubble, and $n$ is the nuclei density per unit volume of liquid.

Using momentum conservation, the following equation is derived:

$$\frac{\partial (\rho \mathbf{U})}{\partial t} + \nabla \cdot (\rho \mathbf{U}\mathbf{U}) - \nabla \cdot \tau = -\nabla p + \rho \mathbf{g} + \mathbf{F} \tag{25.6}$$

**τ,g,F** indicate viscous stress, gravity, and force, respectively.

The 3D model of the bullet is presented in Fig. 25.1, and the computation domain of the bullet is shown in Fig. 25.2a, including four types of boundaries: inlet, outlet, bullet, and symmetry plane. This case is based on a bullet in OpenFOAM, which is in the tutorial directory. The original case used laminar flow as a turbulence model. In this paper, the turbulence model is modified as $k - \mu$ one equation LES model. The radius of the bullet, $d$, is equal to 0.01 m. The distance between the bullet and inlet is $5d$. The distance from the outlet to the bullet is $10d$ and the distance from bullet to the symmetry plane is $5d$, as shown in Fig. 25.2b. Fig. 25.3a and Fig. 25.3b show the mesh generated by snappyHexMesh, a Cartesian meshing tool in

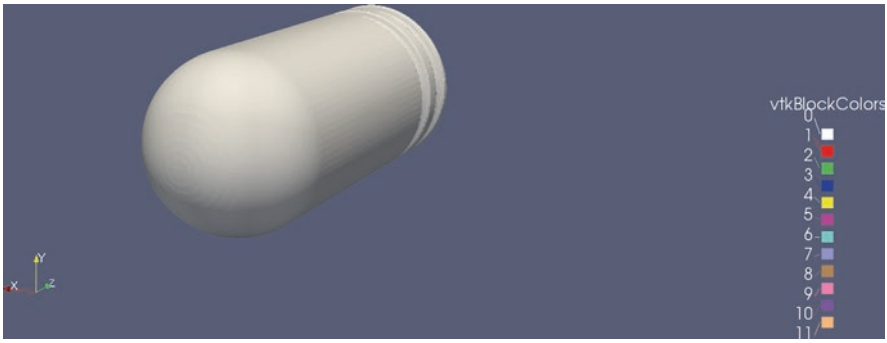


**Fig. 25.1** 3D view of the bullet

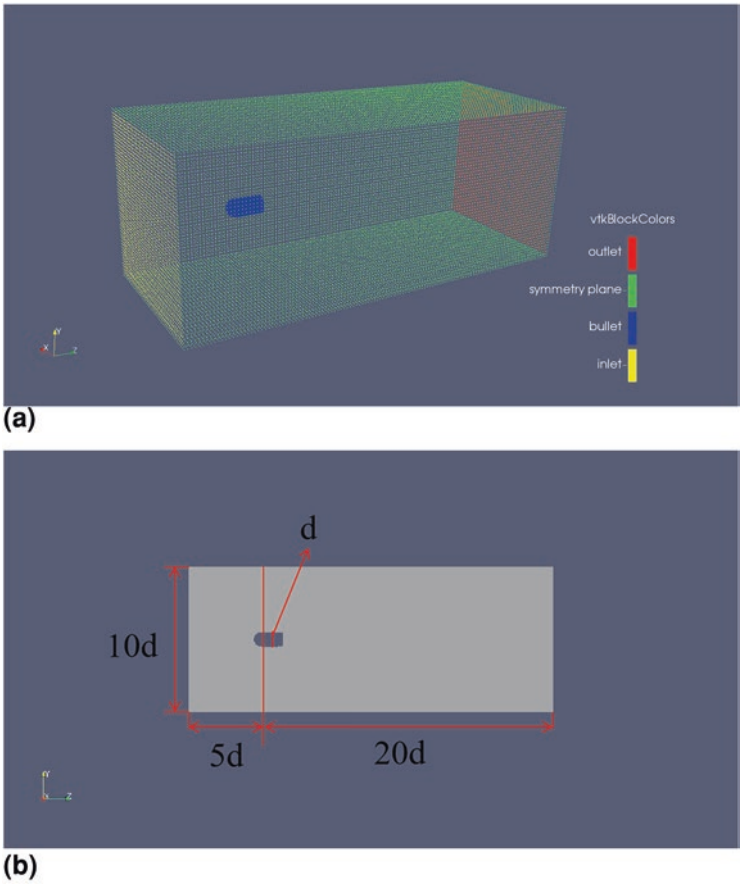


**Fig. 25.2** Computational domain in (**a**) full view (**b**) y–z plane

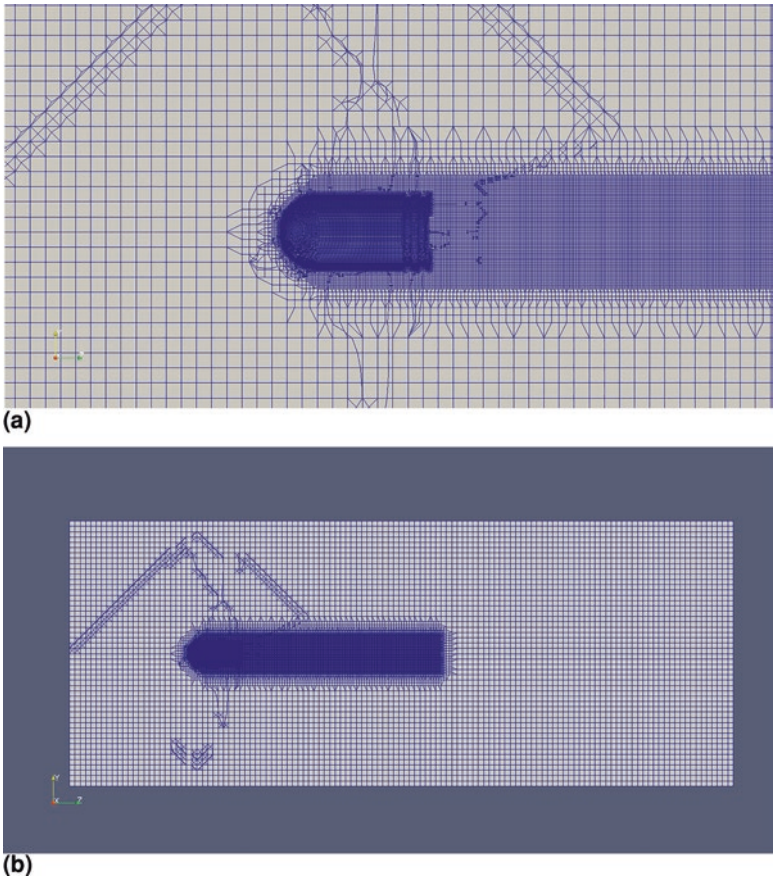


**Fig. 25.3** Grid generated by snappyHexMesh (**a**) full view (**b**) close-up view

OpenFOAM, in full view and close-up view, respectively. The number of cells in this grid is $1.44 \times 10^6$ (Fig. 25.3).

The cavitation number is set to 0.4885, in terms of the following equation:

$$\sigma = \frac{p_\infty - p_{sat}}{\frac{1}{2}\rho_\infty U_\infty^2} \tag{25.7}$$

$\rho_\infty$ is the water density and $U_\infty$ is the flow velocity in the inlet, which is set to 20 m/s. The Reynolds number is $2 \times 10^5$. In order to observe and analyze the evolution of the vorticity field behind the bullet, we use the Omega-Liutex identification method to describe vortex structure. The Omega-Liutex method is enhanced based on the Omega method and the Omega-R method [20–24]; the value of Omega-R is calculated using Eq. (25.8):

$$\Omega_R = \frac{\beta^2}{\alpha^2 + \beta^2 + \varepsilon} \tag{25.8}$$

$\Omega_R$ can be chosen as 0.52 to visualize vortex structure. $\varepsilon$ is empirically defined as a function about $\alpha$ and $\beta$:

$$\varepsilon = b \times \left(\beta^2 - \alpha^2\right)_{\max} \tag{25.9}$$

where $b$ is a small positive number. $\alpha$ and $\beta$ can be written as:

$$\alpha = \frac{1}{2}\sqrt{\left(\frac{\partial V}{\partial Y} - \frac{\partial U}{\partial X}\right)^2 + \left(\frac{\partial V}{\partial X} + \frac{\partial U}{\partial Y}\right)^2} \tag{25.10}$$

$$\beta = \frac{1}{2}\left(\frac{\partial V}{\partial X} - \frac{\partial U}{\partial Y}\right) \tag{25.11}$$

$U$, $V$, $W$ represent the velocity components in the x-, y-, and z-directions, respectively. The derivative of each velocity component can be obtained using the velocity gradient tensor $\nabla\vec{\mathbf{V}}$:

$$\nabla\vec{\mathbf{V}} = \begin{bmatrix} \frac{\partial U}{\partial X}, \frac{\partial U}{\partial Y}, 0 \\ \frac{\partial V}{\partial X}, \frac{\partial V}{\partial Y}, 0 \\ \frac{\partial W}{\partial X}, \frac{\partial W}{\partial Y}, \frac{\partial W}{\partial Z} \end{bmatrix} \tag{25.12}$$

Liu et al. improved Eq. (25.8) and obtained the improved Omega-Liutex identifying method:

$$\tilde{\Omega}_R = \frac{\left(\vec{\omega}\cdot\vec{r}\right)^2}{2\left[\left(\vec{\omega}\cdot\vec{r}\right)^2 - 2\lambda_{ci}^2 + 2\lambda_{cr}^2 + \lambda_r^2\right] + \varepsilon} \tag{25.13}$$

where $\lambda$ represents the eigenvalues of the velocity gradient tensor $\nabla\vec{\mathbf{V}}$. The subscripts *ci*, *cr*, and *r* represent the imaginary part of the complex eigenvalue, the real part of the complex eigenvalue, and the real eigenvalue, respectively. $\vec{\omega}, \vec{r}$ represent the vorticity and the direction of Liutex. $\vec{r}$ has the same direction as the real eigenvector of the velocity gradient tensor $\nabla\vec{\mathbf{V}}$.

## 3 Results and Discussion

The simulation calculates a total of 60-time steps, from 0 s to 0.012 s. The data are written every 0.0002 s. The results show that the whole procedure can be divided into two stages. The first stage is from 0 s to 0.0032 s, during which transient behaviors are significant. The second stage is from 0.0034 s to 0.012 s. At the second stage, the border of cavitation in the flow field gradually stabilizes, and the wake flow behind the bullet is turbulent. In order to elucidate the attributes of the flow field during the two different stages, the velocity field and water volume fraction field are shown in Figs. 25.4 and 25.7, respectively.

Figure 25.4 shows the formation and progression of the re-entrant jet from 0.002 s to 0.0044 s. The contour of the water volume fraction and the vector diagram at the wake region of bullet are presented in Fig. 25.5. At the beginning of the first step, due to the transient behavior of flow, an inception cavitation occurs at the top of the bullet and expands rapidly. In a few time steps, the cavity occupies the entire bullet and extends behind the bullet. At 0.002 s, the growth of the cavity stops and begins to shrink from the tail of the cavity, while the re-entrant jet begins to generate at the end of cavity. At 0.0026 s, the flow at the end of the cavity invades the center of the cavities traveling in the opposite direction to the incoming flow, forming a re-entrant jet structure, as shown in Fig. 25.5. Experimental research reveals that cavitation collapse is mostly caused by re-entrant jet structure. As the re-entrant jet touches and covers the surface of the bullet, the free interface of the cavities begins to become unstable due to interference from the re-entrant jet; the cavity quickly shrinks, which makes the pressure on the surface of the bullet oscillate significantly. After 0.0032s, the attached cavity breaks into small-scale cloud cavity and move downstream. Since the shape of the re-entrant jet is symmetric about the central axis, it can be predicted that the jet and the velocity field are also roughly symmetric about the central axis, as shown in Fig. 25.4.

In order to quantitatively analyze the impact of the reversed flow on the bullet, the drag coefficient curve is calculated and shown in Fig. 25.6. The drag coefficient, $Cd$, is calculated thus:

$$Cd = \frac{F_{drag}}{\frac{1}{2}\rho U_{\infty}^{2} A} \tag{25.14}$$

According to the initial settings for the bullet, the cross-section area of bullet is set to $7.854 \times 10^{-5} m^2$, and $U_\infty$ is set to 20 m/s. The generation of the re-entrant jet occurs in a very short time, and the instantaneous impact between re-entrant jet and the bullet is much greater than the fluctuation in drag force caused by vortex shedding. Comparable phenomena can be perceived for other variables, so we choose the drag coefficient as a typical variable and show it in Fig. 25.6. At about 0.0031 s, the drag coefficient always becomes abruptly much greater than the coefficient at any other time. The huge variation in the drag coefficient mainly takes place between

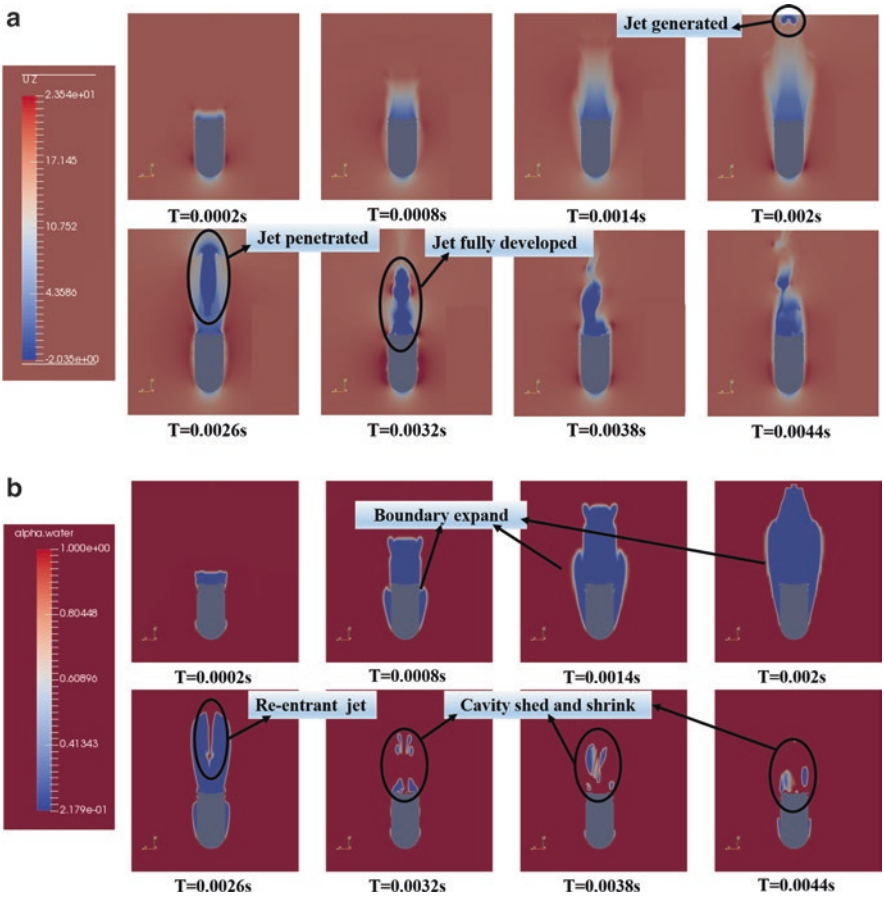


**Fig. 25.4** Flow fields from 0.0002 s to 0.0044 s in (**a**) the z-direction velocity field. The re-entrant jet was generated behind the bullet and quickly penetrated forward until it reached the tail of the bullet. (**b**) Volume fraction of water. The boundary of the cavity expanded rapidly; when it reached its maximum volume, a re-entrant jet was generated in a short time, breaking through the cavity. The cavities at the tail then detached from the bullet and oscillated. A slice in the y–z plane is chosen

0.003 s and 0.0032 s. By comparing Figs. 25.5 and 25.6, it is clear that the fluctuation in drag coefficient is not stimulated by the re-entrant jet contacting the tail of the bullet, but by the collapse of the cavity at the tailing edge of bullet. The cavity is cut off from the center of the re-entrant jet, which produces a strong shock. Then the shock propagates to the bullet. After the cavity has collapsed, the drag coefficient quickly returns to a quasi-stable state, and thereafter, it mainly reflects the vortex shedding effect at the tail of the bullet.

After the re-entrant jet disappears, the cavitation detaches from the bullet and repeats the formation-expansion-collapse cycle at the rear of the bullet for some time. When cavitation no longer appears in about 0.01 s, the cavitation near the

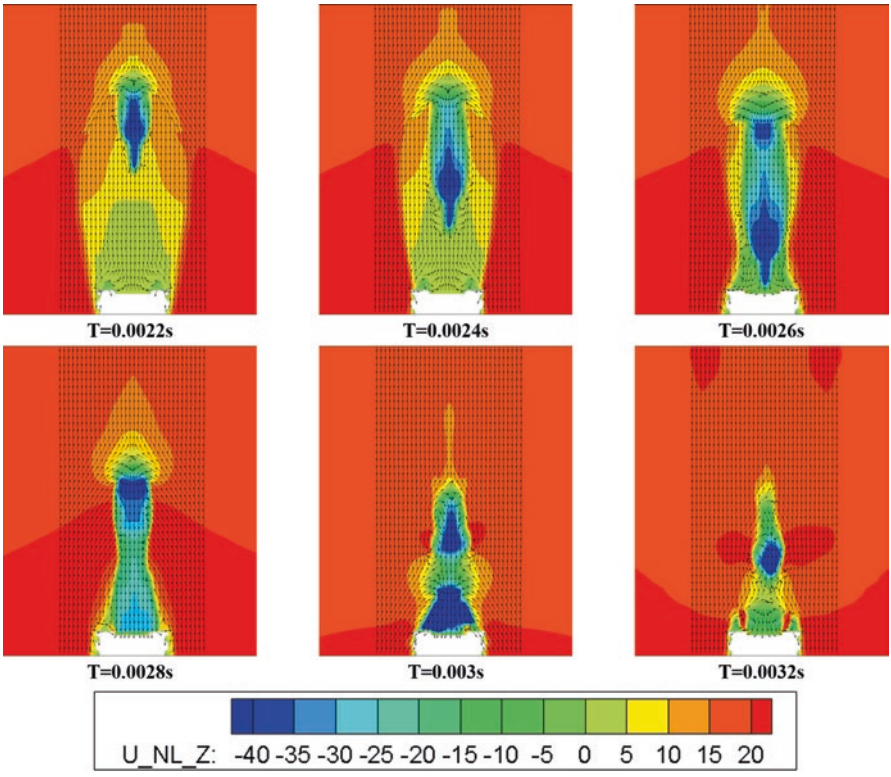


**Fig. 25.5** Evolution of re-entrant jet in 0.001 s. The re-entrant jet originates from a point, which is distanced from about three times the diameter of the bullet and is directed towards the tail of the bullet. A strong fluctuation in velocity occurs after the jet has reached the tail. A slice in the y–z plane is chosen

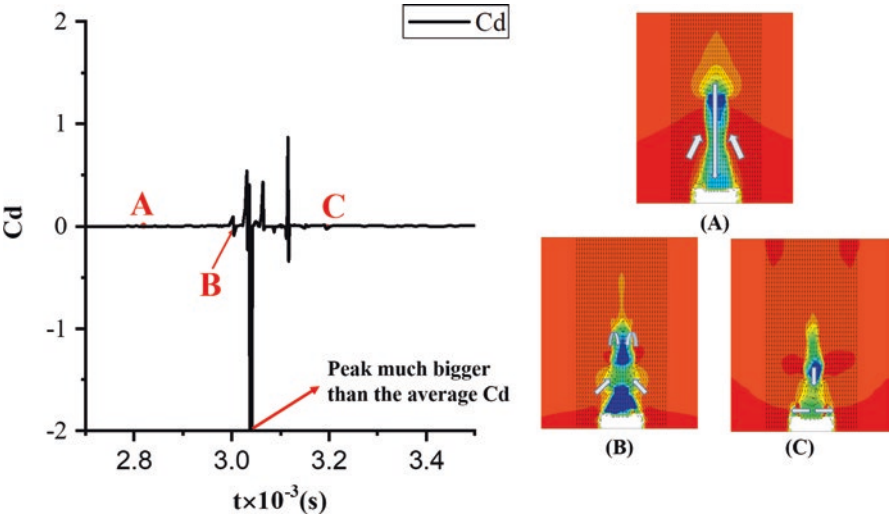


**Fig. 25.6** Drag coefficient curve from 0.0026 s to 0.0038 s. The cavity is cut off from the middle of the cavity, causing a huge fluctuation in drag coefficient

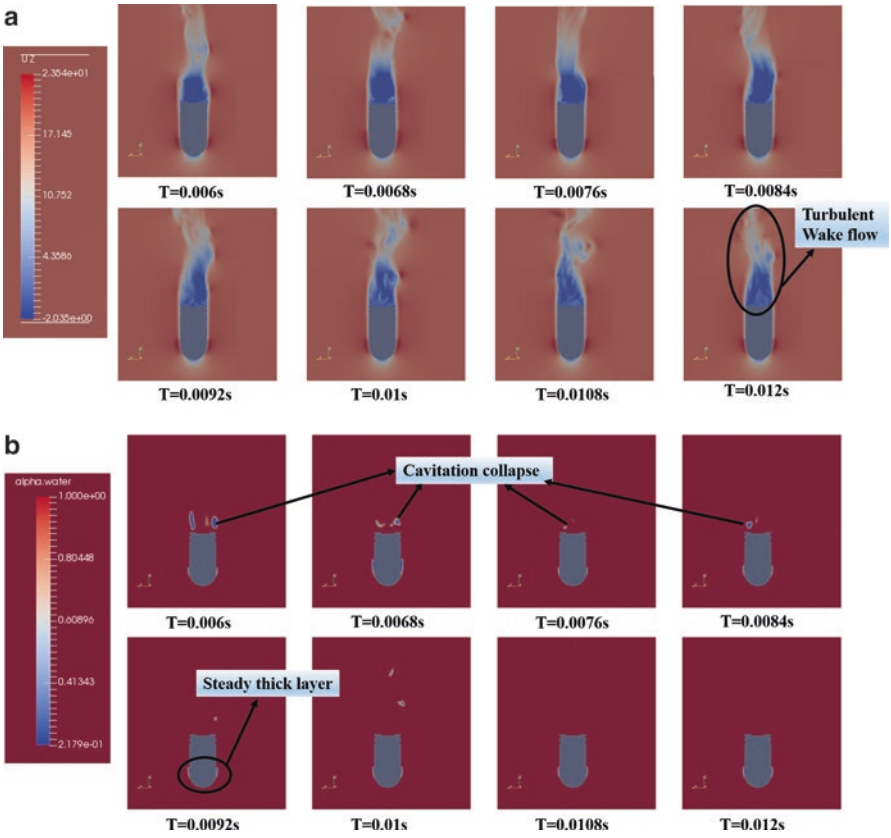


**Fig. 25.7** Physical field from 0.006 s to 0.012 s: (**a**) the z-direction velocity field. The wake-flow regime remained turbulent during the whole process. (**b**) Volume fraction of water. The cavity generated in the former stage collapses over time. The thick layer attached around bullet gradually becomes steady. A slice in the y–z plane is chosen

leading edge of bullet becomes stable. There is no cavitation behind the bullet, and the top of the bullet is covered with a thin layer of cavities. This phenomenon can be clearly seen in Fig. 25.7a, b, which present the features of cavitation in the second stage. Figure 25.7a shows that the velocity field of the bullet after cavitation dissipation is similar to the velocity field for non-cavitation. Due to the use of the LES turbulence model, the wake region of the flow field is turbulent. Figure 25.7b shows the cavity shape in 0.012 s. The reason why the thick cavitation layer around the bullet maintains its stability is because of the cavitation number. The top of the bullet is spherical, which makes it less likely to induce super cavitation. In this case, the cavitation number is not low enough to generate super cavitation, which can wrap around the whole bullet. In this case, the quasi-periodic shedding of cavities does not occur because of the shape of the bullet.

In this paper, we mainly focus on vortex generation when a re-entrant jet develops in a short time. The Omega-Liutex program is applied to describe the evolution of vortices during the formation and elimination of the jet. To understand the relationship between a vortex and cavitation, the volume fraction is plotted in the same figure with an iso-surface obtained using Omega-Liutex in Fig. 25.8. The iso-surface of Omega-Liutex is set to $\tilde{\Omega}_R = 0.52$. In 0.0022 s, the cavity reaches its maximum volume. Since the jet direction is opposite to the direction of the external flow field, a small annular vortex appears at the tip of the jet. The vortex follows the jet and touches the wall of the bullet, and the fluid is forced to change direction, which induces vortex formation at the tail of the bullet. Meanwhile, the vortex that escapes from the bullet draws the fluid on both sides of liquids into the inside of the cavity, cutting the cavity from the center. Tail vortex shedding is induced by the groove near the rear of the bullet. It can be inferred that the groove at the rear end of the bullet has an important influence on the shape of transient cavitation. The groove-induced shedding vortex entrains the fluid into the cavitation, causing the cavitation to break from the center. Compared with the bullet without grooves, the bubbles behind the grooved bullet accelerate the elimination of cavitation. After 0.003 s, the cavity is surrounded by vorticity, which indicates strong vortex motion inside and outside the cavity.

To explore the ability of different methods to extract the vortex structure in cavitating flow, we make a simple comparison of the iso-surface maps obtained using the three different vortex methods for the flow from 0.0022 s to 0.0032 s in Fig. 25.9.

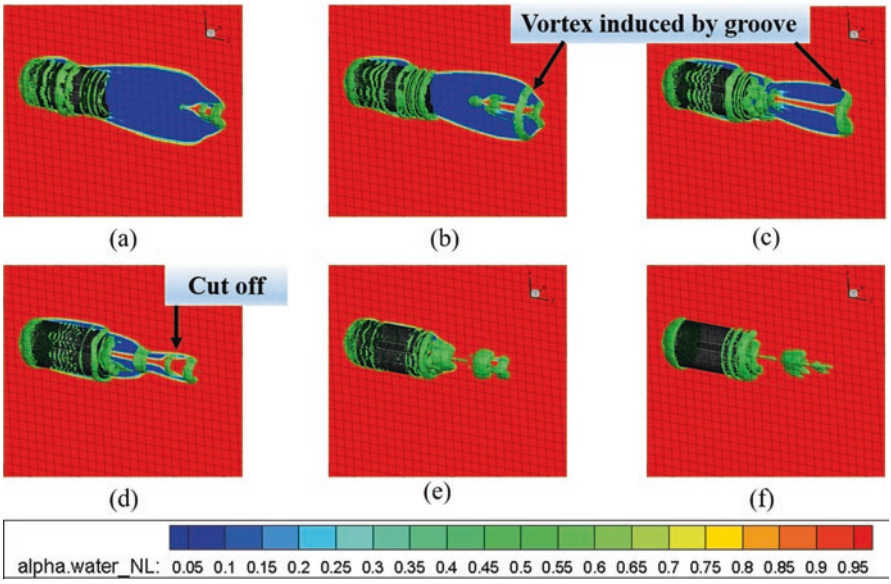


**Fig. 25.8** Iso-surface according to the Omega-Liutex criterion and the contours of the water volume fraction in (**a**) 0.0022 s, (**b**) 0.0024 s, (**c**) 0.0026 s, (**d**) 0.0028 s, (**e**) 0.003 s, and (**f**) 0.0032 s. The contour is plotted in the x-plane. The iso-surface of Omega-Liutex is set to $\tilde{\Omega}_R = 0.52$

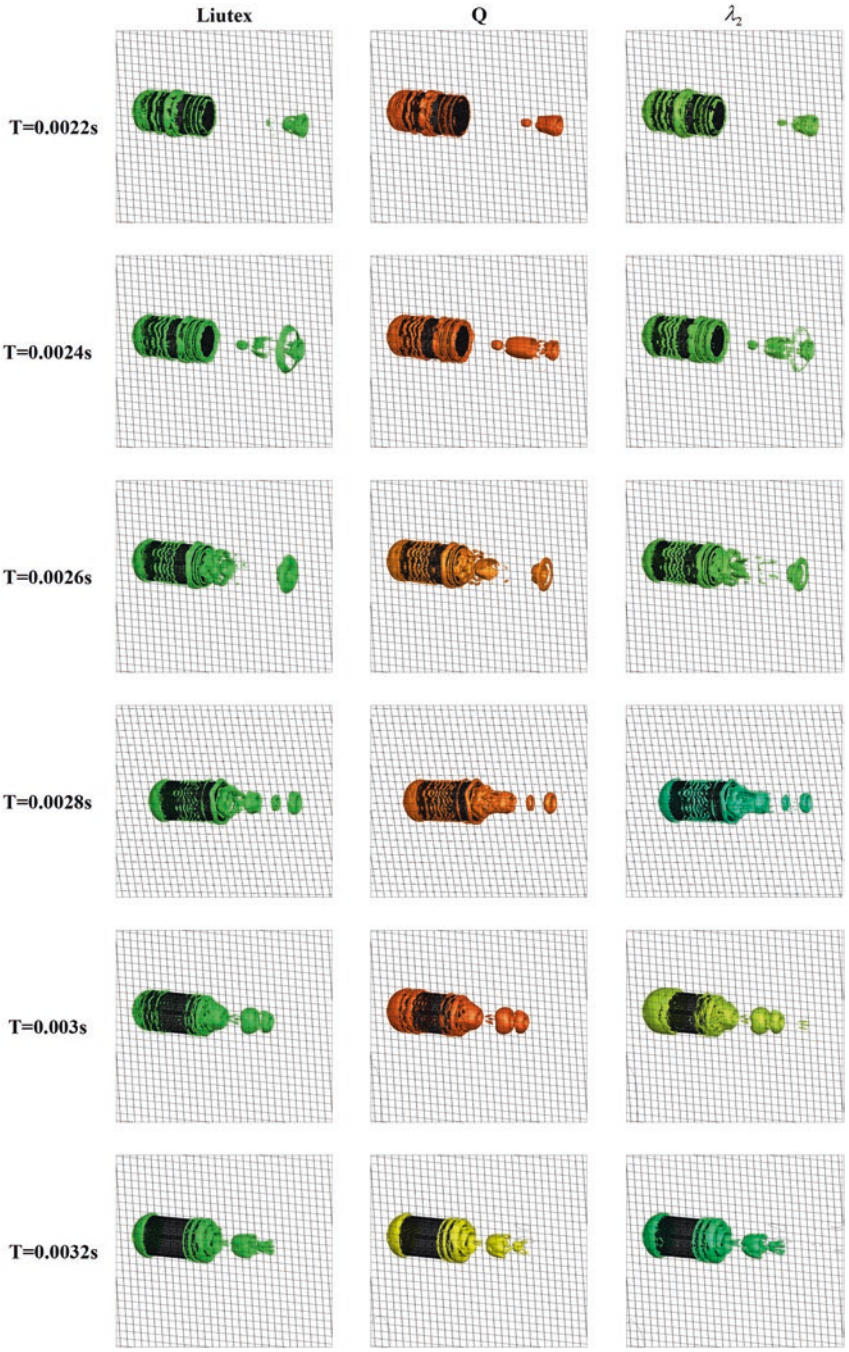


**Fig. 25.9** Different results about various vortex identification using (**a**) Omega-Liutex $\tilde{\Omega}_R = 0.52$ , (**b**) the $\lambda_2$-criterion $\lambda_2 = -5 \times 10^6$, and (**c**) the Q-criterion $Q = 1 \times 10^7$, from 0.0022 s to 0.0032 s

The criterion for adjusting Q and $\lambda_2$ is to make the shape of the shedding vortex at the tail of the bullet approximately the same. The most obvious advantage of Omega-Liutex is that the shape of the vortex can be obtained without modifying the value of the criterion. The $\lambda_2$-criterion and Q-criterion many adjustments to make the vortex structure as clear as possible. Using these criteria (Fig. 25.9), the vortex structure calculated using Omega-Liutex is clearer and the boundary of vortex is more distinct. The iso-surfaces obtained using the $\lambda_2$-criterion and Q-criterion have different degrees of adhesion at the tail of the bullet, meaning the boundary of the vortex structure given by Omega-Liutex is clearer, and the main vortex structure can be better distinguished from the complex flow area. Changing the size of the Omega-Liutex criterion can be done to distinguish between a strong vortex and a weak vortex.

## 4 Conclusions

In this paper, a 10-cm diameter bullet under water is calculated using OpenFOAM. Based on the simulation results, the process is divided into two stages. The transient behavior of the flow field in the first stage is dominant. At the beginning, a large cavity appears and wraps around the whole bullet. As time progresses, the re-entrant jet at the tail of the cavitation is generated and migrates forward, breaking through the cavity and causing the cavity to shrink in a short time. The whole process takes about 0.01 s. The second stage is considered to comprise quasi-steady flow, which is marked by the attachment between the jet and the bullet. After the re-entrant jet has reached the tail of the bullet, the cavity is divided into two parts. In the first part, cavity fluctuates slowly and eventually stabilizes in front of the bullet, forming a thin layer. The second part sheds from the bullet, and the volume of the cavity is quickly attenuated. Soon afterwards, the wake flow of the bullet becomes turbulent. To explore vortex structure during its initial stages, the Omega-Liutex method is utilized to describe a vortex in a wake flow. A comparison between different method is applied and the result shows that Omega-Liutex method has unique advantage in vortex identification. The goal of this paper is to study the phenomenon of a three-dimensional bullet when it is suddenly launched in deep water, and to analyze the vortex structure of the flow problem using Omega-Liutex. The problems similar to this bullet are common in high-speed hydrodynamics. Solving this case about bullet can provide a reference for the modeling and analysis of actual engineering problems. Omega-Liutex provides accurate vortex-structure criteria, providing a reliable tool to better understand cavitating flow fields. This paper studies cavitation around the bullet when it is far away from a free surface. At different depths, the cavitation shape changes, caused by the interaction between the free surface and the bullet; hence this is also worthy of observation and analysis.

**Acknowledgement** This work is accomplished using the code Omega-LiutexUTA, released by Chaoqun Liu at the University of Texas at Arlington. The project is supported by the National Key R&D Program (Grant Nos. 2016YFC0300800, 2016YFC0300802), National Natural Science

Foundation of China (Nos. 11772340 and 11672315), and the Science and Technology on Water Jet Propulsion Laboratory (Grant No. 6142223190101).

## References

1. O. Coutier-Delgosha, R. Fortes-Patella, J.L. Reboud, Evaluation of the turbulence model influence on the numerical simulations of unsteady cavitation. J. Fluid Eng.: Trans. ASME **125**(1), 38–45 (2003)
2. N. Dittakavi, A. Chunekar, S. Frankel, Large Eddy simulation of turbulent-cavitation interactions in a Venturi nozzle. J. Fluid Eng.: Trans. ASME **132**(12), 11 (2010)
3. E. Roohi, A.P. Zahiri, M. Passandideh-Fard, Numerical simulation of cavitation around a two-dimensional hydrofoil using VOF method and LES turbulence model. Appl. Math. Model. **37**(9), 6469–6488 (2013)
4. M. Callenaere, J.P. Franc, J.M. Michel, M. Riondet, The cavitation instability induced by the development of a re-entrant jet. J. Fluid Mech. **444**, 223–256 (2001)
5. C.Q. Liu, Y.Q. Wang, Y. Yang, Z.W. Duan, New omega vortex identification method. Sci. China: Phys. Mech. Astron. **59**(8), 9 (2016)
6. P.-H. Alfredsson, A. Johansson, J. Kim, in *Turbulence Production Near Walls: The Role of Flow Structures with Spanwise Asymmetry*. Stanford Univ., Studying Turbulence Using Numerical Simulation Databases, 2. Proceedings of the 1988 Summer Program, pp. 131–141 (1988)
7. M.S. Chong, A.E. Perry, B.J. Cantwell, A general classification of 3-dimensional flow-fields. Phys. Fluids A: Fluid Dyn. **2**(5), 765–777 (1990)
8. J. Jeong, F. Hussain, On the identification of a vortex. J. Fluid Mech. **285**, 69–94 (1995)
9. X.R. Dong, Y.Q. Wang, X.P. Chen, Y. Dong, Y.N. Zhang, C.Q. Liu, Determination of epsilon for Omega vortex identification method. J. Hydrodyn. **30**(4), 541–548 (2018)
10. Y.N. Zhang, X. Qiu, F.P. Chen, K.H. Liu, Y.N. Zhang, X.R. Dong, C.Q. Liu, A selected review of vortex identification methods with applications. J. Hydrodyn. **30**(5), 767–779 (2018)
11. J.M. Liu, Y.S. Gao, Y.Q. Wang, C.Q. Liu, Objective Omega vortex identification method. J. Hydrodyn. **31**(3), 455–463 (2019)
12. C.Q. Liu, Y.S. Gao, X.R. Dong, Y.Q. Wang, J.M. Liu, Y.N. Zhang, X.S. Cai, N. Gui, Third generation of vortex identification methods: Omega and Liutex/Rortex based systems. J. Hydrodyn. **31**(2), 205–223 (2019)
13. L. Wang, Z.Y. Zheng, W.H. Cai, W.Y. Li, Extension Omega and Omega-Liutex methods applied to identify vortex structures in viscoelastic turbulent flow. J. Hydrodyn. **31**(5), 911–921 (2019)
14. W. Xu, Y. Gao, Y. Deng, J. Liu, C. Liu, An explicit expression for the calculation of the Rortex vector. Phys. Fluids **31**(9) (2019)
15. X. Dong, Y. Gao, C. Liu, New normalized Rortex/vortex identification method. Phys. Fluids **31**(1) (2019)
16. J.M. Liu, Y.S. Gao, C.Q. Liu, An objective version of the Rortex vector for vortex identification. Phys. Fluids **31**(6), 11 (2019)
17. C.C. Wang, Y. Liu, J. Chen, F.Y. Zhang, B. Huang, G.Y. Wang, Cavitation vortex dynamics of unsteady sheet/cloud cavitating flows with shock wave using different vortex identification methods. J. Hydrodyn. **31**(3), 475–494 (2019)
18. S. Xu, X.P. Long, B. Ji, G.B. Li, T. Song, Vortex dynamic characteristics of unsteady tip clearance cavitation in a waterjet pump determined with different vortex identification methods. J. Mech. Sci. Technol. **33**(12), 5901–5912 (2019)
19. Y.F. Wang, W.H. Zhang, X. Cao, H.K. Yang, The applicability of vortex identification methods for complex vortex structures in axial turbine rotor passages. J. Hydrodyn. **31**(4), 700–707 (2019)

20. Y.S. Gao, C.Q. Liu, Rortex and comparison with eigenvalue-based vortex identification criteria. Phys. Fluids **30**(8), 18 (2018)
21. Y.Q. Wang, Y.S. Gao, C.Q. Liu, Letter: Galilean invariance of Rortex. Phys. Fluids **30**(11), 6 (2018)
22. C.Q. Liu, Y.S. Gao, S.L. Tian, X.R. Dong, Rortex—A new vortex vector definition and vorticity tensor and vector decompositions. Phys. Fluids **30**(3), 12 (2018)
23. X.R. Dong, Y.S. Gao, C.Q. Liu, New normalized Rortex/vortex identification method. Phys. Fluids **31**(1), 5 (2019)
24. X.R. Dong, G. Dong, C.Q. Liu, Study on vorticity structures in late flow transition. Phys. Fluids **30**(10), 8 (2018)